Article:
Han, H, Zhang, L, Oghorada, OJK et al. (1 more author) (2020) A delta-connected MMCC-based active power conditioner for unbalanced load compensation and harmonic elimination. International Journal of Electrical Power & Energy Systems, 118. 105811. ISSN 0142-0615

https://doi.org/10.1016/j.ijepes.2019.105811

A Delta-connected MMCC-based Active Power Conditioner for Unbalanced Load Compensation and Harmonic Elimination

Han Huang[a], L. Zhang[b], O.J.K. Oghorada[c], Mingxuan Mao[d]
[a] *College of Engineering, Swansea University, United Kingdom*
[b] *School of Electronic and Electrical Engineering, University of Leeds, United Kingdom*
[c] *Department of Electrical and Information Engineering, Landmark University, Nigeria*
[d] *School of Electronic and Electrical Engineering, Chongqing University, China*
han.huang@swansea.ac.uk

Abstract:

Modular multilevel cascaded converters (MMCC) are seen in medium and high voltage applications and have gained attention from industry. This paper presents new control techniques to improve accuracy and control response speed when applied to a delta-connected MMCC- based Active Power Conditioner used for negative sequence and harmonic current elimination. A novel reference current generation scheme combining a notch filter with Decoupled Double Synchronous Reference Frame (DDSRF) is proposed which can extract the negative sequence and a selection of dominant harmonic currents accurately with the minimum time delay. Fast and accurate tracking the extracted reference current is obtained by using a model-based predictive controller with a derivative reference current term. The control strategy is applied to an experimental delta-connected MMCC-APC and the resultant waveforms are shown and analysed, confirming that the grid current quality after compensation has improved significantly.

Keywords: ***Delta*, *modular multilevel converter, active power filter, unbalanced load, harmonics analysis***

I. INTRODUCTION

Power quality issues are becoming more problematic since modern loads such as computer power supplies, energy efficient light, draw harmonic currents and consume reactive power. Increasing connection of renewable sourced generators to the utility network exacerbates the situation due to their use of power electronic converters for grid interfacing and their unpredictable generating capacity [1, 2], and because they are often connected to only a single system phase. This situation, together with large single-phase loads, such as traction drives, results in a continuing problem of accumulating unbalanced system currents. These may result in voltage imbalance at the point of common coupling, posing threats to system stability and safe operation.

Power converter-based static compensators (STATCOMs) have been shown in recent years to be effective and flexible in not only compensating load reactive current but also mitigating harmonics in real-time [3-5], and so functioning as active power filters. Most are realised as three-phase two-level dc-ac inverters and hence can only handle a few kilovolts when transformers are not used. The development of modular multilevel converters (MMC) [6] has contributed significantly to medium and high voltage power system applications [7, 8], such as HVDC [9-

11] and reactive power compensation [12-14]. An MMCC commonly comprises a chain of full-bridge converters (sub-modules) connected either in single star bridge cell (SSBC) or single delta bridge cell (SDBC) configurations. Having many series-connected sub-modules, the MMCC is easily scalable to higher voltages without requiring a step-up transformer, and it can operate at low switching frequencies while producing lower harmonic outputs. Its modular structure makes it fault tolerant as it can be reprogrammed to bypass a faulty module or to generate reduced voltage [15]. The use of an MMCC for unbalanced current compensation has also been reported, showing that the delta-connected form is more effective than the star-connected counterpart in maintaining MMCC phase limbs voltage balance when compensating unbalanced current [16]. This is because the SSBC requires injection of zero sequence voltage for rebalancing the MMCC inter-cluster power [17-19] while the SDBC requires zero sequence current [20, 21]. The former may cause phase voltages to exceed their rated level, resulting in the SSBC operating in over-modulation mode or even becoming uncontrollable. This, however, does not occur in the SDBC-MMCC, which is therefore chosen for the present work.

Regardless of the converter type, simultaneous compensation of negative sequence, harmonic and reactive current presents the challenge of extracting harmonic and negative sequence current elements as accurately as possible with negligible time delay. Various time and frequency domain techniques have been proposed for harmonic extraction only [22]. Most widely used in frequency domain is the Fast Fourier Transform (FFT) [23], whose accuracy relies on the conditions that the number of samples is an integer power of two over an integer number of cycles, and the waveform is at steady state. This method requires considerable computational effort [24]. Of the two main time domain techniques, one series is based on the instantaneous reactive power theory, proposed by Akagi [25], for harmonics extraction [26-29]. Its drawback is in requiring balanced three-phase grid voltages with no distortion for current calculations. This cannot work for unbalanced loads since the voltage under this condition may be distorted or imbalanced, hence affecting the accuracy of harmonic current calculation. The other series is the synchronous reference frames (SRF) proposed by Divan [30] which has the advantage of only requiring three measured phase currents for computation, but transformation of measured currents to the *d-q* rotating reference frame needs phase locking on to the grid voltage which may be inaccurate due to grid voltage distortion. In addition, if the load is unbalanced the transformed *d-q* current elements contain additional cross coupling components due to imbalance may affect the accuracy in harmonic compensation.

This paper proposes two extraction schemes which can simultaneously identify harmonic and unbalanced current elements; both use the Decoupled Double Synchronous Reference Frame (DDSRF) [31]. The first combines a stationary reference notch filter for dominant harmonic detection and the DDSRF for imbalance current extraction. The second extends the SRF scheme to both negative and positive current sequences and applies low pass filters to both components. The two techniques are compared in this paper and relative advantages

of the notch filter-based method are found. Cancellation of load current unbalance and distortion also relies on fast responding control scheme, hence the paper also proposes a model-based predictive controller with a derivative reference current term. The proposed techniques are validated using an experimental delta-connected MMCC-APC, with a total of six sub-modules, to compensate the unbalanced and distorted current of a network. The resultant current waveforms and comparisons are presented and analysed.

Section II of the paper describes the system configuration investigated, with unbalanced and nonlinear loads, and the structure of the compensating MMCC-APC. Section III analyses the *d-q* components of the unbalanced fundamental current, and symmetrical and asymmetrical harmonics currents. The proposed harmonics and negative sequence current extraction schemes are illustrated and compared in Section IV. The current control, together with summary MMCC capacitor voltage balancing schemes, is discussed in Section V. Simulation results are finally presented and compared with experiment.

II. SYSTEM CONFIGURATION

The distribution system used for developing and validating the MMCC-APC is shown in Fig. 1. Bus 1 is connected to a three-phase ac voltage source representing the power grid; Bus 2 is the Point of Common Coupling (PCC), connected with the MMCC-APC and a load bus. There are two loads connected on the load bus: a three-phase thyristor rectifier load representing the nonlinear and distorting current generating source, and a three-phase R-L load with variable impedance to emulate unbalanced load.

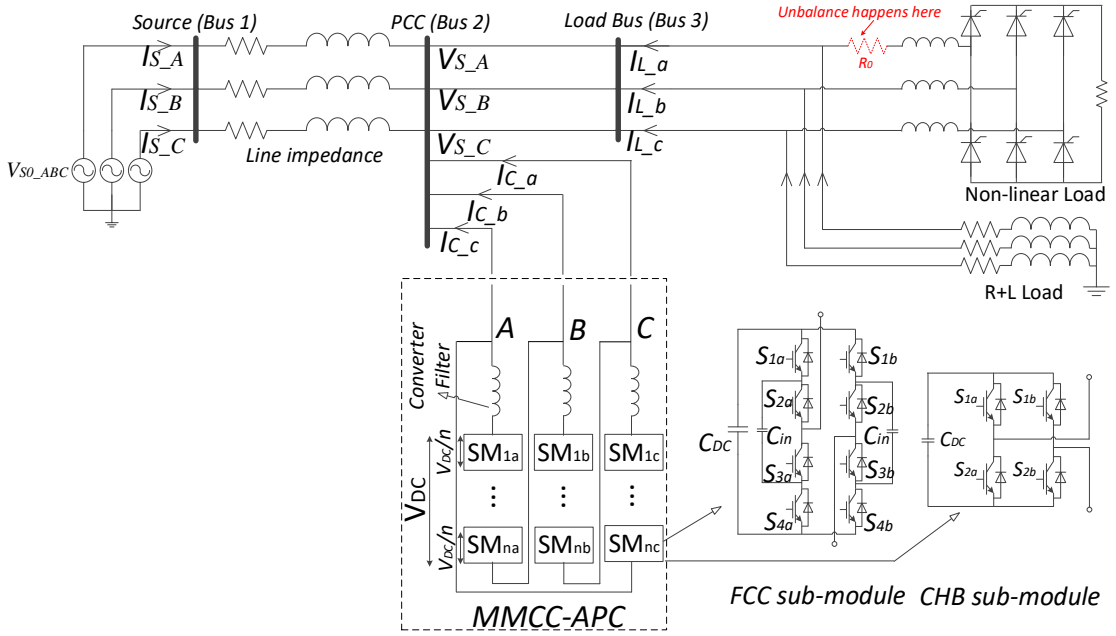

Fig. 1 System circuit configuration diagram

The MMCC-APC, presented in Fig. 1, consists of three phase limbs (AB, BC and CA) in delta connection and connected to the grid line through a low-pass R-L filter. Each of the phase limbs is composed of a chain of

submodules (SMs) which are either a 2-level H-bridge (HB) or a 3-level full-bridge flying capacitor converter (FCC). In this work the latter was chosen for its higher number of voltage levels and increased availability of switching states per module. The two limbs of an FCC share a common dc-bus capacitor $\boldsymbol{C_{DC}}$, each having two complementary switch pairs and a flying capacitor $\boldsymbol{C_{in}}$ connected between them. It synthesises 5 voltage levels, i.e. $\pm V_{DC}, \pm\frac{1}{2}V_{DC}$ and 0. Both FCC and HB topologies have been reported in STATCOM and active filtering applications [16, 32].

III. ANALYSIS OF UNBALANCED CURRENT

A key requirement for MMCC-APC to mitigate the unbalanced and distorted load current is that it can extract the current elements to be injected into the grid with high precision and short time delay. It should also supply the required amount of reactive power to maintain near unity power factor at PCC. Analysis of current elements under unbalanced load conditions is necessary to determine the current to be injected; one is the unequal fundamental phase currents due to over or light loading of one or two phases with mainly sinusoidal current drawing loads, and the other is both fundamental and harmonic current imbalance. The latter is most common, often caused by distribution line impedance differences due to faults, loading one or two phases with excessive power electronic converter-controlled load, and asymmetric connections of single-phase grid-tie converters for renewable sourced generators.

A. Unbalanced Fundamental Current

Unbalanced three-phase current can be decomposed, according to Fortescue's theorem, to three balanced symmetrical phasor systems, namely positive sequence, negative sequence and zero sequence as given by (1). To measure the degree of current imbalance a parameter $\boldsymbol{K_{ir}} = \frac{I^-}{I^+}$ is defined where I^- is the negative (-ve) sequence component in the current in RMS and I^+ is the positive (+ve) sequence in RMS. When I^-= 0, $\boldsymbol{K_{ir}}$=0, load current is balanced; on the other hand, when $\boldsymbol{K_{ir}}$=1, or 100%, I^-=I^+ and load current is severely unbalanced. So the load three-phase current is

$$i_{ABC} = I^+ + I^- + I^0 = i^+\begin{bmatrix}\cos(\omega t+\varphi_{Ip})\\ \cos(\omega t-\frac{2\pi}{3}+\varphi_{Ip})\\ \cos(\omega t+\frac{2\pi}{3}+\varphi_{Ip})\end{bmatrix} + i^-\begin{bmatrix}\cos(\omega t+\varphi_{In})\\ \cos(\omega t+\frac{2\pi}{3}+\varphi_{In})\\ \cos(\omega t-\frac{2\pi}{3}+\varphi_{In})\end{bmatrix} + i^0\begin{bmatrix}\cos(\omega t+\varphi_{I0})\\ \cos(\omega t+\varphi_{I0})\\ \cos(\omega t+\varphi_{I0})\end{bmatrix} \quad (1)$$

Using the Clarke transformation the α-β expression using is given as

$$i_{\alpha\beta} = \begin{bmatrix}i_\alpha\\ i_\beta\end{bmatrix} = [T_{\alpha\beta}]i_{ABC} = I^+\begin{bmatrix}\cos(\omega t+\varphi_{Ip})\\ \sin(\omega t+\varphi_{Ip})\end{bmatrix} + I^-\begin{bmatrix}\cos(-\omega t+\varphi_{In})\\ \sin(-\omega t+\varphi_{In})\end{bmatrix} \quad (2)$$

where $[T_{\alpha\beta}] = \frac{2}{3}\begin{bmatrix} 1 & -\frac{1}{2} & -\frac{1}{2} \\ 0 & \frac{\sqrt{3}}{2} & -\frac{\sqrt{3}}{2} \end{bmatrix}$, with no neutral connection, zero sequence is cancelled.

Projection of $i_{\alpha\beta}$ on positive and negative synchronous reference frames (SRF), rotating at $+\omega$ and $-\omega$ respectively leads to i_{dq}^{+} and i_{dq}^{-} which are expressed as

$$i_{dq}^{+} = \begin{bmatrix} i_d^{+} \\ i_q^{+} \end{bmatrix} = [T_{dq}{}^{+1}] i_{\alpha\beta} = I_1^{+} \begin{bmatrix} \cos\varphi_{Ip} \\ \sin\varphi_{Ip} \end{bmatrix} + I_1^{-} \begin{bmatrix} \cos 2\omega t & \sin 2\omega t \\ -\sin 2\omega t & \cos 2\omega t \end{bmatrix} \begin{bmatrix} \cos\varphi_{In} \\ \sin\varphi_{In} \end{bmatrix} \quad \text{and} \qquad (3)$$

$$i_{dq}^{-} = \begin{bmatrix} i_d^{-} \\ i_q^{-} \end{bmatrix} = [T_{dq}{}^{-1}] i_{\alpha\beta} = I_1^{-} \begin{bmatrix} \cos\varphi_{In} \\ \sin\varphi_{In} \end{bmatrix} + I_1^{+} \begin{bmatrix} \cos 2\omega t & -\sin 2\omega t \\ \sin 2\omega t & \cos 2\omega t \end{bmatrix} \begin{bmatrix} \cos\varphi_{Ip} \\ \sin\varphi_{Ip} \end{bmatrix} \qquad (4)$$

where $[T_{dq}{}^{+1}] = \begin{bmatrix} \cos\omega t & \sin\omega t \\ -\sin\omega t & \cos\omega t \end{bmatrix} = [T_{dq}{}^{-1}]^T$.

From above expressions, one can see the cross coupling between *d-q* axis signals of both SRFs. The positive *d-q* components contain an ac element at twice the fundamental frequency, ω, with the amplitudes equal to the negative sequence dc term. Likewise the negative *d-q* components have an ac element of 2ω with the same magnitude as the positive dc term. The cross coupling of –ve fundamental to +ve elements at the SRF creates challenges to harmonic extraction, since 2ω terms need to be eliminated. Clearly to eliminate unbalanced current the injected current needs to have not only the negative sequence element but also 2ω positive sequence element.

B. Balanced and Unbalanced Harmonic Currents

Balanced Harmonic Quantities: these are equal in magnitude across the three phases and can be categorised according to their harmonic order (h =1,2,3…) into positive sequence (6h+1), negative sequence (6h-1) and zero sequence (6h-3). Note that even harmonics are disregarded since they arise from asymmetry between positive and negative half-cycles and are negligible in most power systems. The lowest few three-phase odd order harmonic currents, such as 3rd, 5th and 7th, can be expressed as (5)-(7).

$$i_{3A} = I_3 \cos 3\omega t\,, i_{3B} = I_3 \cos 3(\omega t - \tfrac{2\pi}{3}) = I_3 \cos 3\omega t, i_{3C} = I_3 \cos 3(\omega t + \tfrac{2\pi}{3}) = I_3 \cos 3\omega t \qquad (5)$$

$$i_{5A} = I_5 \cos 5\omega t\,, i_{5B} = I_5 \cos 5\left(\omega t - \tfrac{2\pi}{3}\right) = I_5 \cos\left(5\omega t + \tfrac{2\pi}{3}\right), i_{5C} = I_5 \cos 5(\omega t + \tfrac{2\pi}{3}) = I_5 \cos(5\omega t - \tfrac{2\pi}{3}) \qquad (6)$$

$$i_{7A} = I_7 \cos 7\omega t\,, i_{7B} = I_7 \cos 7\left(\omega t - \tfrac{2\pi}{3}\right) = I_7 \cos\left(7\omega t - \tfrac{2\pi}{3}\right), i_{7C} = I_7 \cos 7(\omega t + \tfrac{2\pi}{3}) = I_7 \cos(7\omega t + \tfrac{2\pi}{3}) \qquad (7)$$

From (5) the symmetric 3rd harmonic (6h-3) set is the zero sequence having three phase currents which are all in phase with one another and have equal magnitude. Hence they exist as a zero sequence element only, and cancel each other on phase line. In fact this applies to all triplen harmonics. Their synchronous reference frame

translations, I_0, I_d and I_q components can be given as (8). The derivation through *d-q-0* transformation equations is seen in the appendix.

$$i_0 = I_3 \cos 3\omega t,\ i_d = 0,\ i_q = 0 \tag{8}$$

Only zero sequence i_0 exists and varies sinusoidally at three times the fundamental frequency with amplitude equals to I_3, no i_d and i_q present.

The 5th harmonic has three phase currents with the same magnitude and the same phase differences between each other, but the phase sequence is the reverse of that of the applied voltage, hence it is a symmetrical negative sequence (6h-1) vector. The synchronous reference frame element i_0 and the *d-q* components are given by

$$i_0 = 0, i_d = I_5 \sin(6\omega t),\ i_q = I_5 \cos(6\omega t) \tag{9}$$

From above i_0 equates to zero, the d-component of current i_d varies sinusoidally at 6 times of the fundamental frequency with magnitude equals to I_5, and i_q also varies sinusoidally at the same frequency and amplitude as i_d, but phase shifted by 90◦.

For the 7th harmonic its three phase currents also have the same magnitude and the phase differences between each other are equal, but the phase sequence is positive, so it exists as a positive sequence vector. The transformation to SRF *d-q-0* components are given in the appendix.

$$i_0 = 0, i_d = -I_7 \sin(6\omega t),\ i_q = I_7 \cos(6\omega t) \tag{10}$$

It is clear from the above symmetrical positive sequence harmonics translate to equal magnitude i_d and i_q components with frequency decreased by 1 owing to the matched rotational direction of the synchronous frame. The zero sequence component equals to zero.

Unbalanced Harmonic Quantities: When the magnitudes of an individual harmonic in each phase are not equal they may consist of positive, negative and zero sequence components regardless of their orders. For example, a set of unbalanced 3rd harmonics with phase A and B oscillate at three-times of the fundamental frequency and unity magnitude, and phase C magnitude is zero. Their transformation equations to SRF *d-q-0* components are as

$$i_0 = \frac{2}{3} I_3 \cos 3\omega t \tag{11}$$

$$i_d = \frac{1}{3} I_3 \left(\sin(4\omega t) - \sin(2\omega t) + \sin\left(4\omega t - \frac{2\pi}{3}\right) - \sin(2\omega t + \frac{2\pi}{3}) \right) \tag{12}$$

$$i_q = \frac{1}{3} I_3 \left(\cos(4\omega t) + \cos(2\omega t) + \cos\left(4\omega t - \frac{2\pi}{3}\right) + \cos\left(2\omega t + \frac{2\pi}{3}\right) \right) \tag{13}$$

Clearly the zero component oscillates at the original third frequency but both *d* and *q* components are non-zero quantities containing two frequency harmonics (3+1) and (3-1), either side of the original 3rd order harmonic. These two frequencies represent the +ve and –ve sequences components of the unbalanced 3rd order set respectively. This example shows that for a set of unbalanced harmonic, its synchronous reference frame translation contains multiple frequency elements which must be extracted for cancellation.

IV. NEGATIVE SEQUENCE AND HARMONIC CURRENT EXTRACTION METHODS

The negative sequence and harmonic current elements can be extracted from the measured load current. The two extraction schemes for data processing use either a notch-filter employing Stationary Reference Frame plus Decoupled Double Synchronous Reference Frame (DDSRF), or a low-pass filter relying on the Synchronous Reference Frame (SRF).

A. Notch Filter Based Extraction

1) Harmonics Extraction

The transfer function of a simple Notch Filter (NF) is a second order element given as

$$T(s)_{NF} = \frac{s^2+\omega_0^2}{s^2+2\sigma\omega_0 s+\omega_0^2} \quad (14)$$

where ω_0 defines the centre frequency required to be stopped; for example ω_0 =1571 rad/s for notching the 5th harmonic. Fig. 2 illustrates the Bode plot of the 5th harmonic NF log magnitude which approaches -∞ at 250 Hz; the damping ratio σ is smaller for a narrower notch. In this case σ around 0.05 gives a narrow notch most suitable for stopping the 5th harmonic.

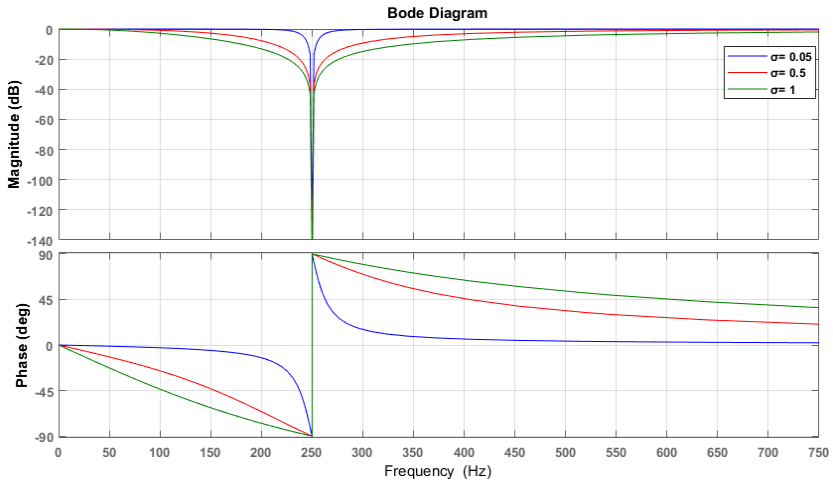

Fig. 2 Bode plot of a NF with ω_0=1571 rad/s

The analysis of the unbalanced and distorted load current has shown that the 3rd, 5th, 7th, 9th and 11th are the most significant major harmonics which are required to be suppressed. To extract these elements simultaneously, 5 cascaded NFs as shown in Fig. 3(b) are used, with their corresponding ω_0 values in (14) as $n\omega_1 = n \times 50 \times 2\pi, (n = 3,5,7,9,11)$. The corresponding transfer function of the cascaded notch filter is given as

$$T(s)_{CNF} = \prod_{n=3,5,7,9,11} \frac{s^2+(n\omega_1)^2}{s^2+2\sigma_n(n\omega_1)s+(n\omega_1)^2} \quad (15)$$

where $\sigma_n \leq 0.05$ in order to give narrow enough notches to stop all the main harmonics. The corresponding Bode plot of the filter is as shown in Fig. 3(a). Using this NF to process each measured phase current samples which are in stationary reference frame, and grouped in ***A*** as shown in Fig. 3(b), the output, grouped in ***B***, are the three phase unbalanced fundamental current plus higher order harmonics which are negligible. Subtracting ***B*** from the original measured current, the resultant three phase currents, grouped in ***C***, are those harmonic elements, I_{href_abc}, selected for elimination.

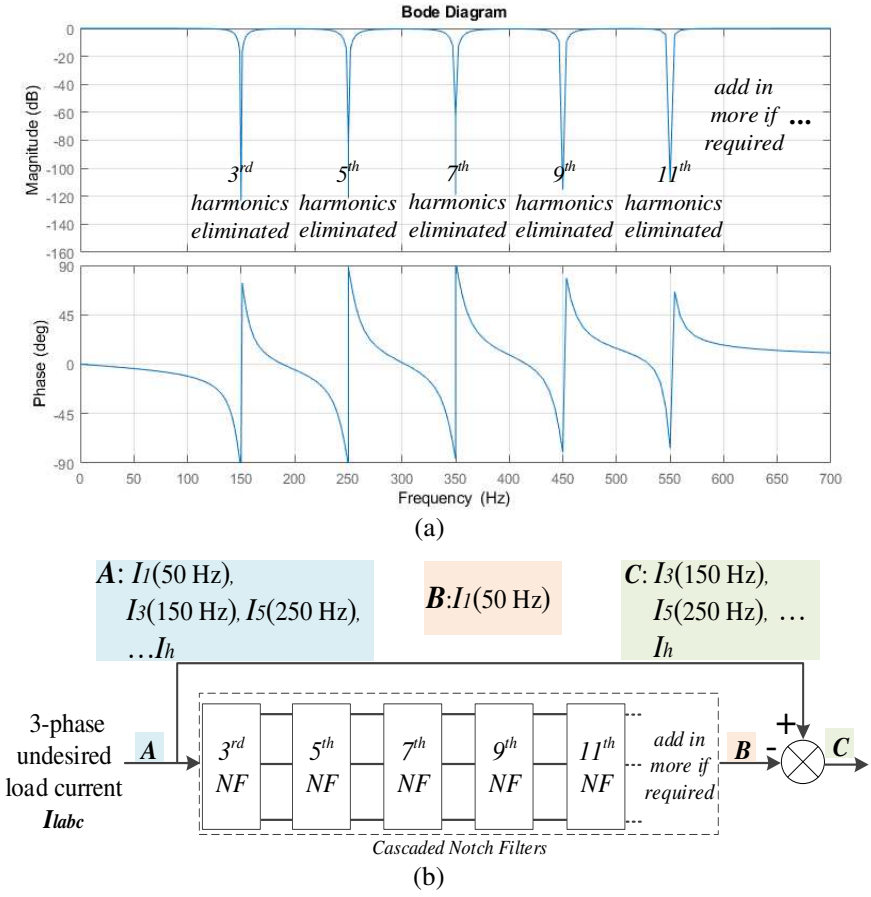

Fig. 3 (a)Corresponding NFs bode plot and (b) Cascaded NF block diagram

2) Negative Sequence Current Extraction

The unbalanced 3-phase currents in Group ***B*** as indicated in Fig. 3(b) are further processed to extract negative sequence and reactive current elements. Assuming no neutral line, these currents can be decomposed to the balanced positive (+ve) and negative (-ve) sequence sets as

$$i_{ABC} = I^+ + I^- = i^+ \begin{bmatrix} \cos(\omega t + \varphi_{Ip}) \\ \cos(\omega t - \frac{2\pi}{3} + \varphi_{Ip}) \\ \cos(\omega t + \frac{2\pi}{3} + \varphi_{Ip}) \end{bmatrix} + i^- \begin{bmatrix} \cos(\omega t + \varphi_{In}) \\ \cos(\omega t + \frac{2\pi}{3} + \varphi_{In}) \\ \cos(\omega t - \frac{2\pi}{3} + \varphi_{In}) \end{bmatrix} \quad (16)$$

To measure the degree of current imbalance a parameter $\boldsymbol{K_{ir}} = \frac{I^-}{I^+}$ is defined where I^- is the –ve sequence component in the current in RMS and I^+ is the +ve sequence in RMS. When $I^- = 0$, $\boldsymbol{K_{ir}}$=0, load current is balanced; on the other hand, when $\boldsymbol{K_{ir}}$=1, or 100%, $I^- = I^+$ and load current is severely unbalanced.

With +θ and –θ identified from PCC voltage, using Clarke and Park transformations the decomposed currents can be projected on the +ve and -ve synchronous reference frames (SRF), rotating at $+\omega$ and $-\omega$ respectively leads to i_{dq}^+ and i_{dq}^- which are expressed as

$$i_{dq}^+ = \begin{bmatrix} i_d^+ \\ i_q^+ \end{bmatrix} = \left[T_{dq}{}^{+1}\right] i_{\alpha\beta} = I_1^+ \begin{bmatrix} \cos\varphi_{Ip} \\ \sin\varphi_{Ip} \end{bmatrix} + I_1^- \begin{bmatrix} \cos 2\omega t & \sin 2\omega t \\ -\sin 2\omega t & \cos 2\omega t \end{bmatrix} \begin{bmatrix} \cos\varphi_{In} \\ \sin\varphi_{In} \end{bmatrix} \quad (17)$$

and

$$i_{dq}^- = \begin{bmatrix} i_d^- \\ i_q^- \end{bmatrix} = \left[T_{dq}{}^{-1}\right] i_{\alpha\beta} = I_1^- \begin{bmatrix} \cos\varphi_{In} \\ \sin\varphi_{In} \end{bmatrix} + I_1^+ \begin{bmatrix} \cos 2\omega t & -\sin 2\omega t \\ \sin 2\omega t & \cos 2\omega t \end{bmatrix} \begin{bmatrix} \cos\varphi_{Ip} \\ \sin\varphi_{Ip} \end{bmatrix} \quad (18)$$

where $\left[T_{dq}{}^{+1}\right] = \begin{bmatrix} \cos\omega t & \sin\omega t \\ -\sin\omega t & \cos\omega t \end{bmatrix} = \left[T_{dq}{}^{-1}\right]^T$.

The *d-q* current elements, i_{dq}^+ and i_{dq}^-, obtained are now predominantly fundamental elements, but they contain their respective 2ω cross coupling terms according to (17) and (18) which need to be taken out in order to extract the fundamental reactive current elements $I_{1\_q}^+$ and $I_{1\_dq}^-$. This can be achieved by using the DDSRF [31]. As shown in Fig. 4, using the i_{dq}^+ and i_{dq}^- to subtract their respective 2ω cross coupling terms, the first terms on the right-hand-side of (17) and (18) can be extracted.

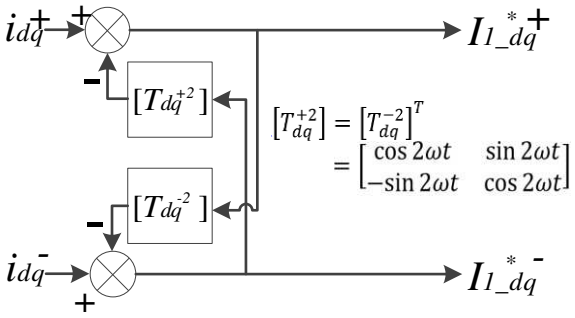

Fig. 4 Block diagram of Decoupled Double Synchronous Reference Frame

The final dc current elements are $I_{1\_dq}^+$ and $I_{1\_dq}^-$, except $I_{1\_d}^+$ which is the load real current component, the rest three are summed to form a part of the reference current, as shown in Fig. 5. There is one more element, I_{dc}, required to be in the reference current, this is derived from the module average voltage control loop to maintain capacitor voltage balance.

All fundamental reference current elements are then inverse Park transformed back to the *a-b-c* stationary frame to give I_{1ref_abc}, this is summed up with the I_{href_abc} and become the reference current signal $I^*_{c\_abc}$ for converter current control as shown in Fig. 5.

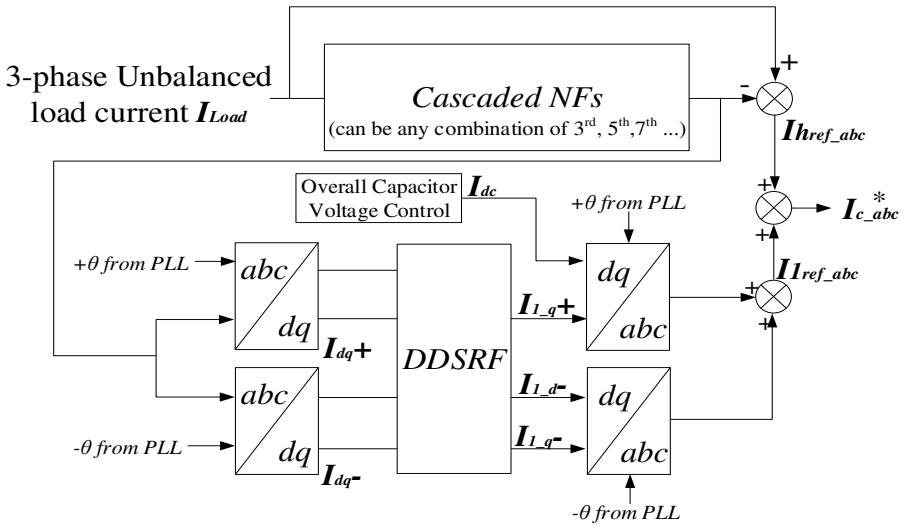

Fig. 5 Block diagram of harmonic and negative sequence current extraction scheme

B. Low Pass Filter Based Extraction

In this operation the negative sequence current extraction is applied in the same way as for the NF-based method described in the Subsection IV-A above. Extraction of harmonic currents in i^+_{dq} uses a Low Pass Filter (LPF), as shown in Fig. 6.

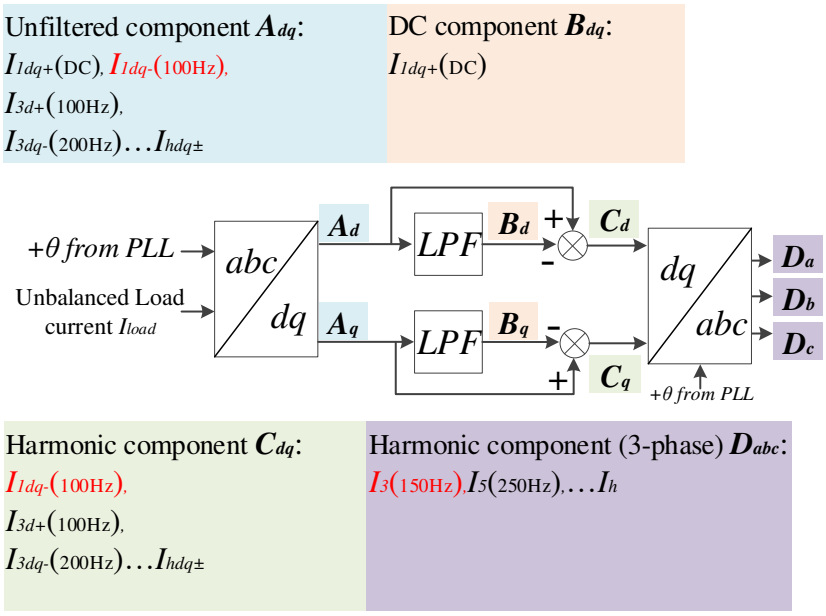

Fig. 6 LPF harmonic current extraction block diagram

Note the transfer function of LPF is $LPF(s) = \frac{\omega_f}{s+\omega_f}$, the cut-off frequency $f_c = \frac{\omega_f}{2\pi}$, with a roll-off of 20 dB/decade, which must be sufficiently low to enable eliminating the 2nd harmonic but high enough to maintain a

fast response speed. However, this scheme cannot distinguish the unbalanced fundamental current and 3rd harmonic component when they transformed into *d-q* format, which makes the final extracted reference containing extra 3rd harmonic component, as shown in the Fig. 6 red highlighted part. This becomes a potential drawback of the LPF-based scheme and more analysis will be given in the next subsection.

Subsequently, only $\bar{i}^{*}_{1\_dq}{}^{+}$ are subtracted from the original measured currents, giving the harmonic components $I^{*}_{h\_d}$ and $I^{*}_{h\_q}$ which are set as a part of the reference current. The total reference current should also add the negative sequence current elements $i^{-}_{1\_dq}$ and the reactive current $i^{+}_{1\_q}$ as illustrated in Fig. 7.

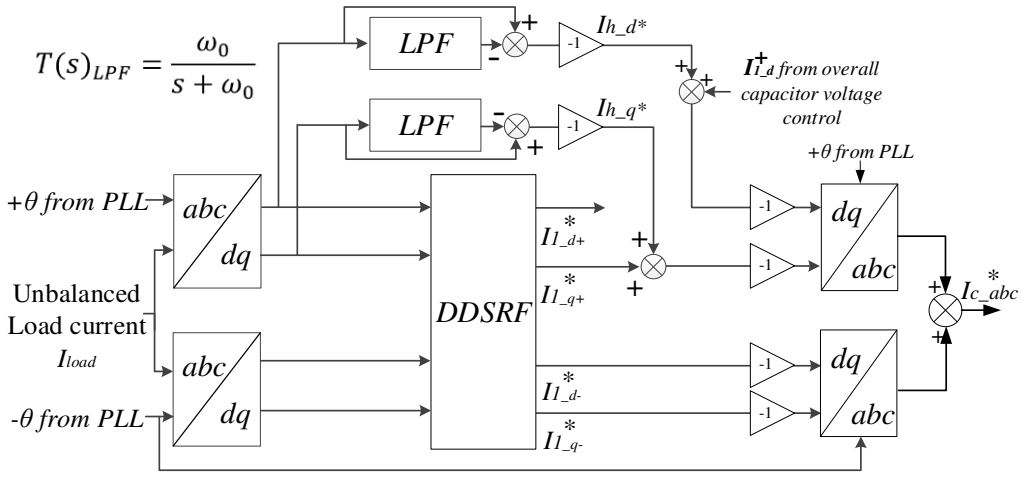

Fig. 7 LPF-based extraction scheme

C. Comparison with LPF Harmonic Current Extraction Schemes

Fig. 8 compares the three phase PCC currents after harmonic extraction and their respective THDs using the above two different schemes. It can be seen that the NF-based scheme (red) can extract the harmonics more accurately (THDs are 1%-5% lower) and faster (around 50 ms) than the LPF-based scheme (blue). This is particularly evident from 3-phase current THDs; at steady states the THDs from the NF scheme are lower showing it extracts higher percentages of harmonics than its counterpart. During transient states, when α changes from 0° to 30° and 30° to 60°, the NF-based scheme is faster to respond to the change and the NF controlled currents settle down quicker.

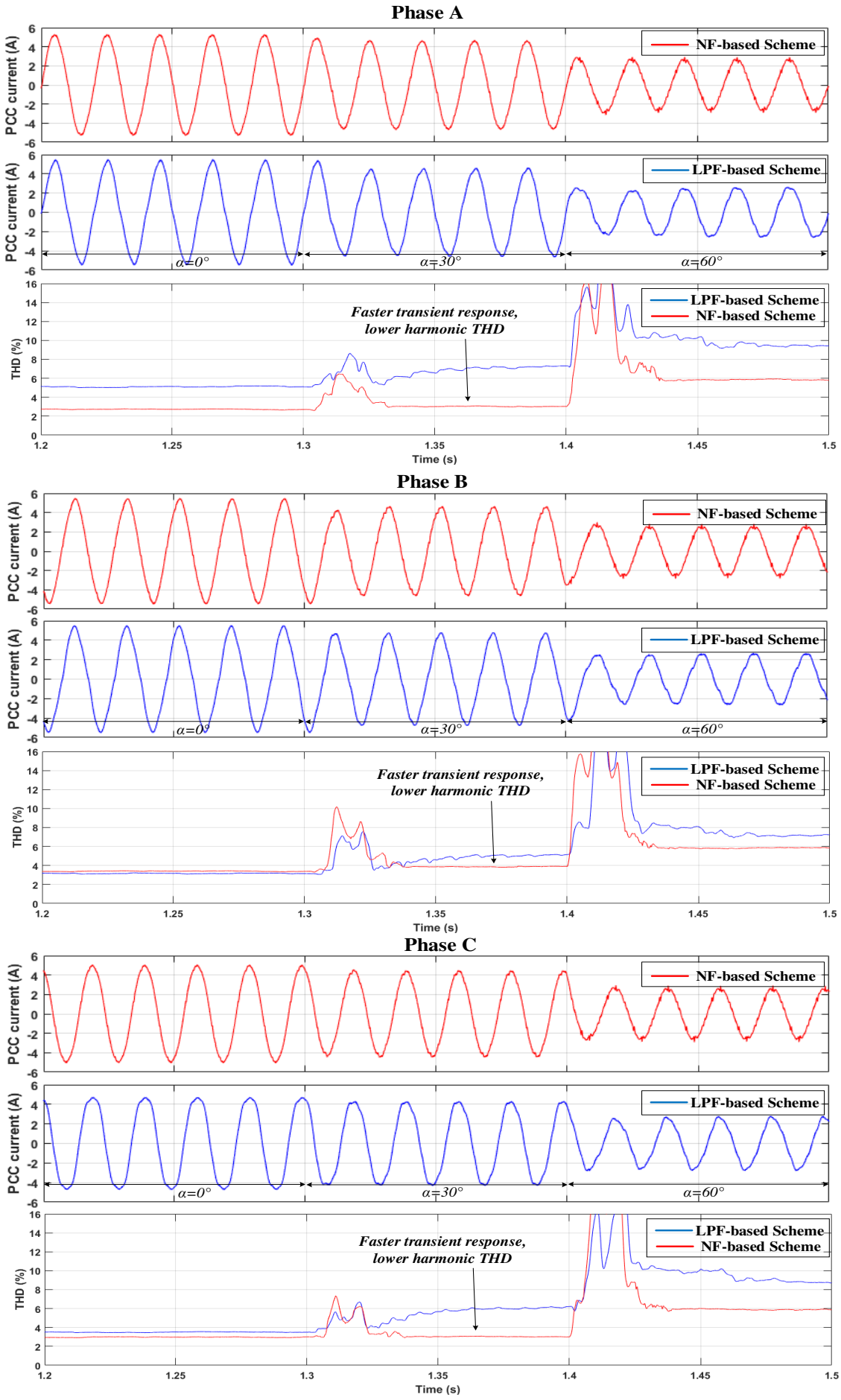

Fig. 8 Three-phase compensated currents and their THD comparison under NF and LPF-based schemes

Fig. 9 compares the most significant low order harmonic current components remaining in the three-phase load currents measured at Bus 2 in the system shown in Fig. 1 after harmonic extraction using either the NF or LPF-based schemes. The load currents vary due to firing angle α changing from 0°, 30° and 60° respectively. It shows that the 3rd order harmonics in three phases are around 308% higher (α=0°) when using the LPF-based scheme, and even increased to 681% higher when α changes to 60°, which significant affect the 3-phase PCC current quality. On the other hand, the harmonic components are all effectively reduced by using the NF-based scheme.

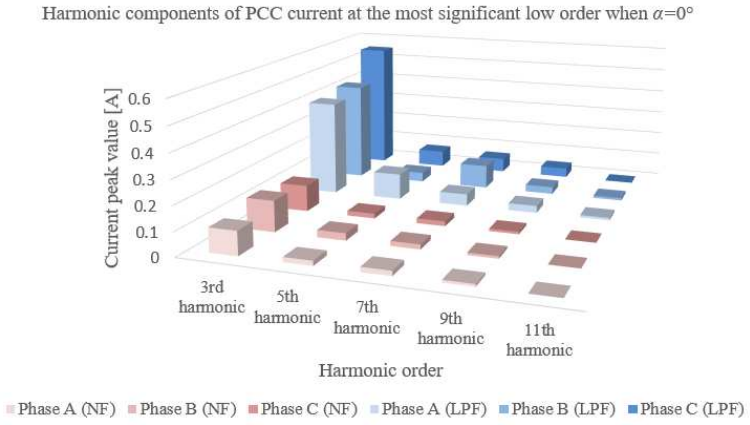

(a)

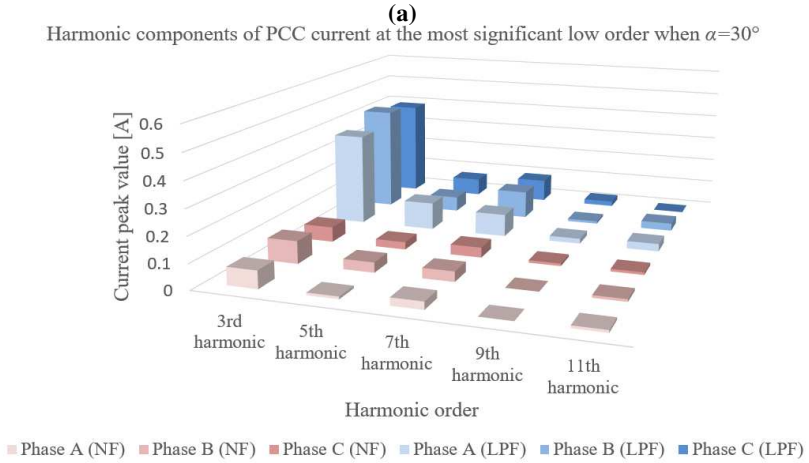

(b)

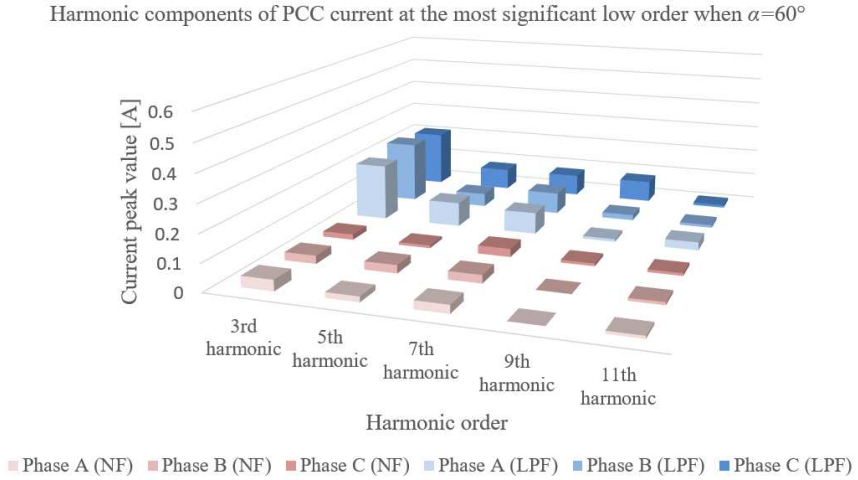

(c)

Fig. 9 Comparison of harmonic current components using NF and LPF-based scheme when (a) α = 0°; (b) α = 30°; (c) α = 60°

Thus in comparison to the LPF based scheme, the NF-based extraction scheme has the following advantages:

- ***Higher speed in reference current elimination***: the NF-based scheme concentrates on a few lower-order major harmonics in the load current; the bandwidth of the lowest element is higher than that when using the LPF; hence it incurs less time delay between the original and extracted currents compared to the LPF, and enables the controller to eliminate harmonics rapidly.
- ***Flexibility in harmonic element selection***: in the cascaded NF block one can adjust notch frequencies flexibly to suit the harmonics needing elimination in a particular case. For example, when the current fundamental element is unbalanced while its harmonics are symmetrical as described in Section III, the triplen harmonics and their multiples are absent, and hence the 3rd and 9th band-stop filters can be removed from the cascaded NF block.
- ***Higher extracting precision***: with the LPF-based scheme, the 3rd harmonics are transformed into 2nd order via the Park transformation, which also converts unbalanced fundamental current into the 2nd harmonic as shown in Fig. 6. These two 2nd order elements will add vectorially and cause the converter to inject redundant ($i_{1\_dq}^{-}$ in 100Hz) 3rd harmonic into the grid and result in harmonic extraction error. Using NFs can extract the harmonics in the *a-b-c* stationary reference frame directly and thus avoid this issue.

V. CONTROL AND MODULATION SCHEME FOR MMCC-BASED ACTIVE POWER CONDITIONER

A. Predictive Current Control

The reference current extracted which is in stationary reference frame is then applied to a predictive controller in order to make the MMCC-APC to generate corresponding converter current. However accurate current control may not be obtained by the conventional predictive control scheme. This is due to the extracted harmonic current having high rate-of-change values and is time varying, while there is a 1-sample time delay imposed to the control action stemming from the predictive controller's inherent feature, also the use of LPF-based extraction scheme with low bandwidth for harmonic reference current extraction incurs further delay. An example reference current tracking and the corresponding PCC current are shown in Fig. 10. There is clearly a tracking error between the converter and reference currents especially when load current changes sharply, which causes the three-phase PCC current to be distorted.

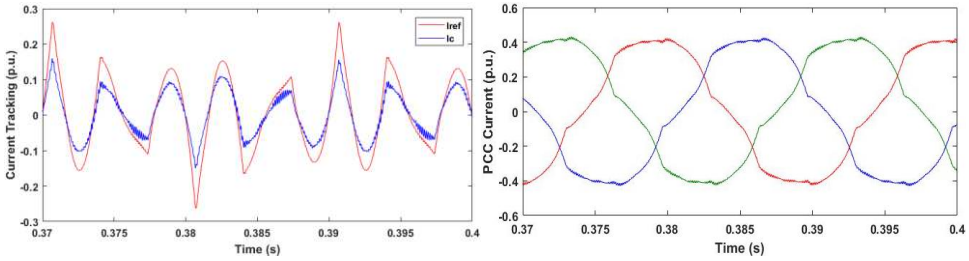

(a) **(b)**

Fig. 10(a) Simulated converter current reference tracking waveforms; (b) Three-phase PCC current

The effective way is by adding a derivative term in the conventional predictive control algorithm. This is realised by using the reference current at the last sample and comparing its value with that at the current sample; the derivative value of the reference current can be obtained by evaluating the ratio of the difference between them over the sample time. Adding this derivative term to the original reference value a new reference current for the compensator is obtained, as shown below.

$$\vec{i_c^*}'(k) = \vec{i_c^*}(k) + \tau \frac{\vec{i_c^*}(k) - \vec{i_c^*}(k-1)}{T_s} \tag{19}$$

The equation shows a coefficient τ being used to scale the derivative term. The value of τ needs to be carefully chosen for achieving the desired compensation effect; in this study, through trial and error, $0<\tau<0.1$ was found to be sufficient in all cases. Thus, the MMCC reference voltage vector equation can be expressed as (20).

$$\overrightarrow{V_{cm}}^*(k) = \overrightarrow{V_{sm}}(k) - \left[\frac{L_c}{T_s} + \tau\frac{L_c}{T_s^2}\right]\overrightarrow{i_{cm}^*}(k) + \tau\frac{L_c}{T_s^2} \times \overrightarrow{i_{cm}^*}(k-1) + \left[\frac{L_c}{T_s} - R_c\right]\overrightarrow{i_{cm}}(k) \tag{20}$$

where *m* represents phases A, B and C.

Applying this control algorithm, the reference current tracking is as shown in Fig. 11. Fig. 11(b) shows the corrected PCC current. All these waveforms show significant improvement as compared to those in Fig. 10.

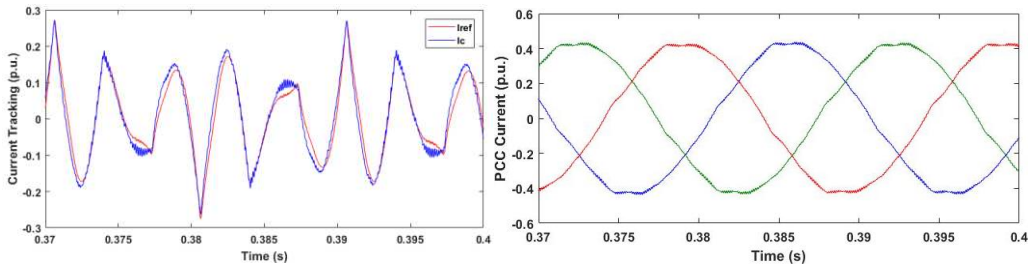

(a) **(b)**

Fig. 11(a) Simulated converter current reference tracking waveforms; (b) Three-phase PCC current with modification ($\tau = 0.02$)

B. Capacitor Voltage Balance Control

An MMCC-based converter can be used to compensate unbalanced and harmonic load current, which results in two types of dc-link capacitor voltage imbalance: inter-phase imbalance and intra-phase imbalance. The former

is due to power flowing in MMCC three phase limbs unequally, and the stacked sub-modules in each phase having their module capacitors isolated from each other preventing active power exchanges between phases. The latter is caused by unequal charging and discharging currents to MMCC module capacitors. Methods for preventing dc voltage drift away for both cases have been developed and presented in detail in the literatures [16, 33]. A summary is given below only for the completeness of control scheme.

1) Inter-phase-Cluster Voltage Balancing Control

For a SDBC-MMCC a zero sequence current is applied which circulates in the delta-configured three-phase limbs to cancel the power terms due to imbalanced voltage and current, hence bring phase cluster voltage balance. Derivation is given in [16] and the resultant instantaneous zero sequence current needs to be converted into voltage command v_{com} through a proportional gain, as shown in (21). Consequently the v_{com} is then applied as a part of the reference voltage to control the converter switches.

$$v_{com} = K_{Pio}\left[-\frac{(i_{ab}+i_{bc}+i_{ca})}{3} + I_o \sin(\omega t + \varphi_o)\right] \tag{21}$$

2) Overall Capacitor Voltage Control

This controls voltages of all sub-module capacitors within a phase cluster due to converter losses using the well-known and applied feedback dc voltage control. In an MMCC the average voltage of all sub-modules is evaluated as

$$V_{DC\_avg} = \frac{V_{DC\_a}+V_{DC\_b}+V_{DC\_c}}{3} \tag{22}$$

where $V_{DC\_(abc)} = \frac{1}{n_{SM}} \sum_{i=1}^{n_{SM}} V_{DC\_i(abc)}$ and n_{SM} equals the number of submodule in each phase limb.

The resultant values are applied to a PI controller with the reference voltage V_{DC_ref}, which is determined by the nominal dc voltage value for each submodule. The output reference current signal $I_{dc\_ref}^{+}$ from this controller then is added onto the converter positive sequence reference current.

C. Carrier Permutation Phase Shift-PWM

The Phase Shift-Pulse Width Modulation (PS-PWM) scheme has been widely used for MMCCs to synthesise the desired waveforms in switch-mode operation [34], and relies on having multiple triangular carrier waves phase shifted relative to each other by a fixed angle. The number of carriers is the number of distinct output voltage levels n (from 0 to the peak level) minus 1 and the phase shift is 180°/(n-1). This method enables the MMCC to approximate the reference waveform with reduced and higher frequency harmonics at a given switching frequency. However, in the application to compensate load harmonic currents, the converter phase voltage waveforms are distorted, causing submodule capacitor voltages to drift away from their nominal levels. In this

work a Carrier Permutation PS-PWM scheme [35] is adopted to prevent capacitor voltage drifting. It still uses multiple triangle carriers, but instead of applying each of them in a fixed sequence cycle by cycle they are cyclically permuted one position forward at the end of each fundamental cycle. This enables the charging and discharging current through the submodule capacitors to vary from cycle to cycle according to the reference voltage pattern, and hence greatly reduces the voltage drift.

After all the reference current generated, the model predictive controller is applied for the converter current to follow the reference. The overall MMCC-APC control scheme is shown in Fig. 12, which comprises three essential parts; the reference current extraction and feedback current control part, the inter-cluster voltage balancing control and the intra-cluster capacitor voltage control.

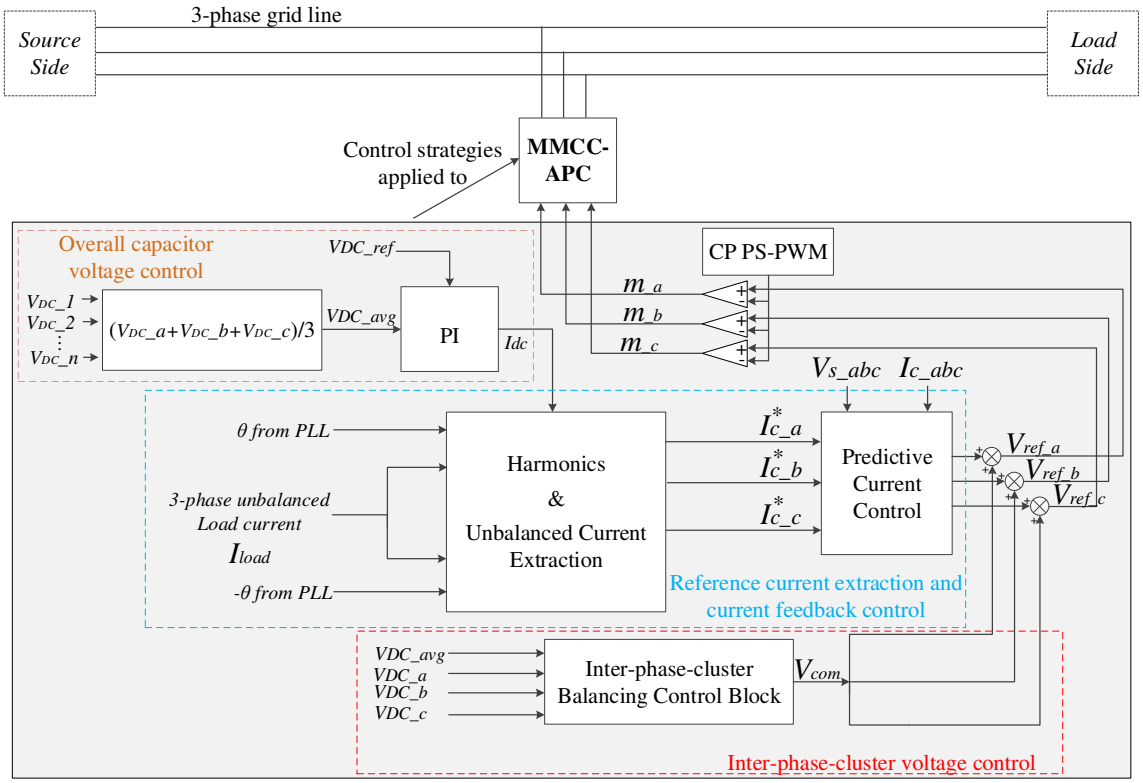

Fig. 12 MMCC-APC control strategies blocks diagram

VI. SIMULATION RESULTS

To validate the effectiveness of the proposed control schemes, the MMCC-APC and corresponding system are simulated through SIMULINK/MATLAB, using the system parameters listed in Table I; the three-phase source voltage rating is 80 V, 50 Hz; the delta-connected MMCC contains two submodules in each phase, while the module capacitor per submodule operates at 80 V. The level of load current imbalance is varied by the rheostat value R_0. Fig. 13(a) shows the three-phase currents measured at the PCC, load, and converter terminals respectively. It can be seen that using the predictive current control the MMCC can eliminate 3-phase harmonic current with high rate-of-change, maintaining the current at the PCC well balanced and sinusoidal, even though

the load current is distorted and unbalanced. Fig. 13(b) shows the injecting zero sequence current and MMCC line voltage. The zero sequence current is distorted due to the harmonics compensation, but it only circulates within the converter phases to ensure the cluster active power balanced and has no effect on the grid current. Hence, the converter line voltage is balanced and shows 9 voltage levels distinct from peak to peak.

Table I Simulated and Experimental component parameters

Components		Value
Source Side	3-phase Source Max. voltage V_{s0}	*2.4 kVA (80 V, 10A)*
Distribution Line	Aluminium PI TX line (d=10mm, l=1.1km)	R_{line} *= 0.5 Ω;* L_{line} *= 2mH*
Load Side	3-Phase Diode Rectifier R+L Load Unbalanced resistor	*1.2 kVA (80 V, 5A)* R_{dc} *= 20Ω;* L_{ac} *= 8.3mH* R_l *= 10Ω;* L_l *= 48mH* R_0 *= 5Ω for* K_{ir}*= 0.4*
Converter Side	RL Filter DC capacitor in each sub-module Switching frequency	*1.4 kVA (240 V, 5A)* R_c *= 1.59Ω;* L_c *= 2mH* V_{dc}*= 400V;* C_{dc}*= 1.12 mF (utilized at 80V)* *1 kHZ*

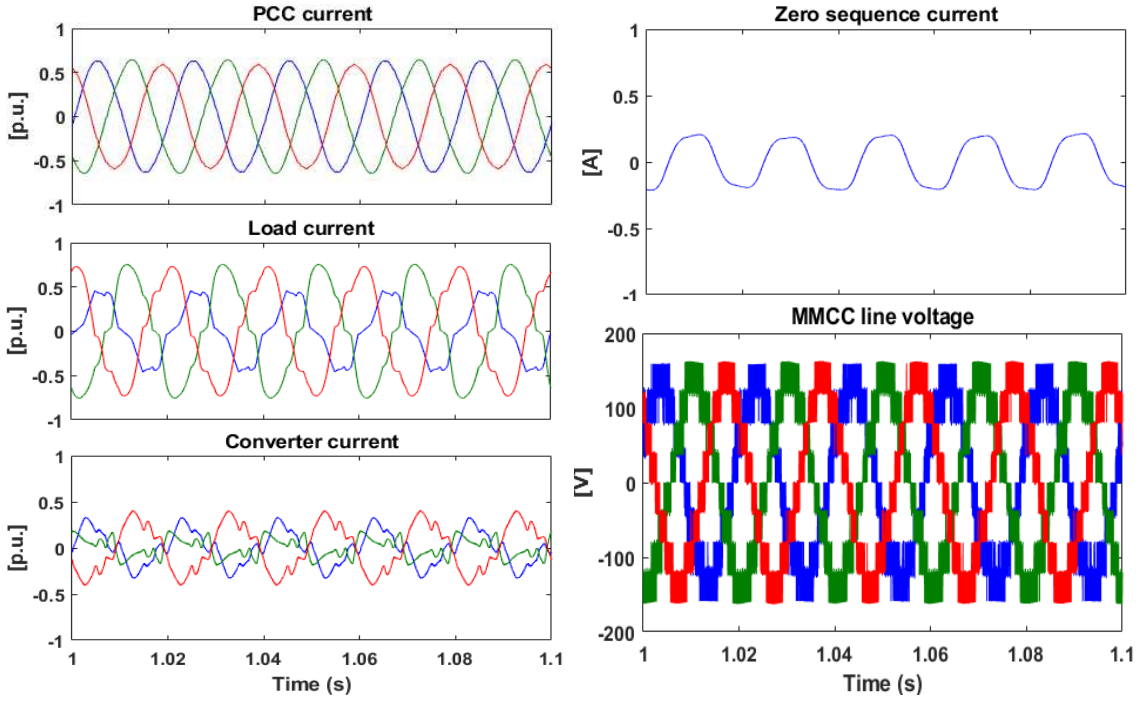

(a) (b)

Fig. 13 (a) Simulated 3-phase current under MMCC-APC compensation; (b)Zero sequence current and MMCC-APC three-phase line voltage

The 3-phase PCC current harmonics spectrum after and before MMCC compensation are shown in Fig. 14. Its fundamental elements become rebalanced after compensation and the several most significant low order harmonics are also eliminated.

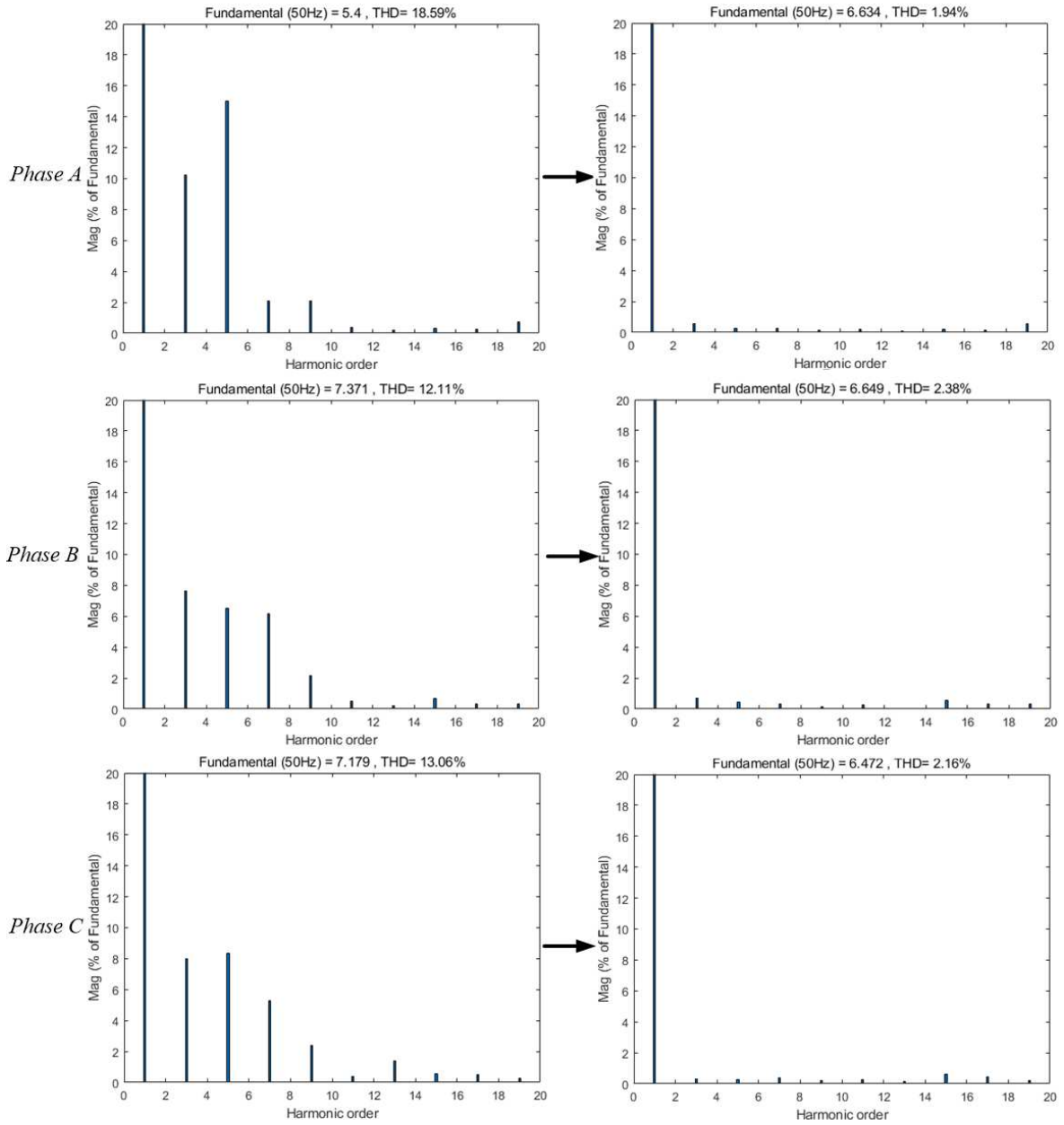

Fig. 14 3-phase current harmonics spectrum before & after MMCC compensation

The results of the system operating behaviour are shown in Fig. 15. As can be seen, the device is not in action between 0< t <0.1sec, the PCC current waveforms $\boldsymbol{I_{Sabc}}$ are unbalanced and not in phase with the voltage $\boldsymbol{V_{Sabc}}$. From t >0.1 sec, APC is turned on to perform reactive current compensation and harmonic elimination, resulting in the PCC current being in phase with the PCC voltage and sinusoidal, but phase currents are still unbalanced. In this case the converter three-phase current $\boldsymbol{I_{Cabc}}$ is increased and distorted. From t>0.2sec, the device is set to supply load required reactive current, eliminate harmonics as well as rebalancing the 3-phase current. During 0.2<t<0.7sec when K_{ir} changes from 0.4 to 0.7, the PCC current is shown to be balanced and sinusoidal. The converter current is naturally increased and unbalanced. The zero sequence current $\boldsymbol{I_0}$ is gradually increased to balance the MMCC cluster active power. In a consequence, the 6 module dc voltages are keep maintained in their nominal value.

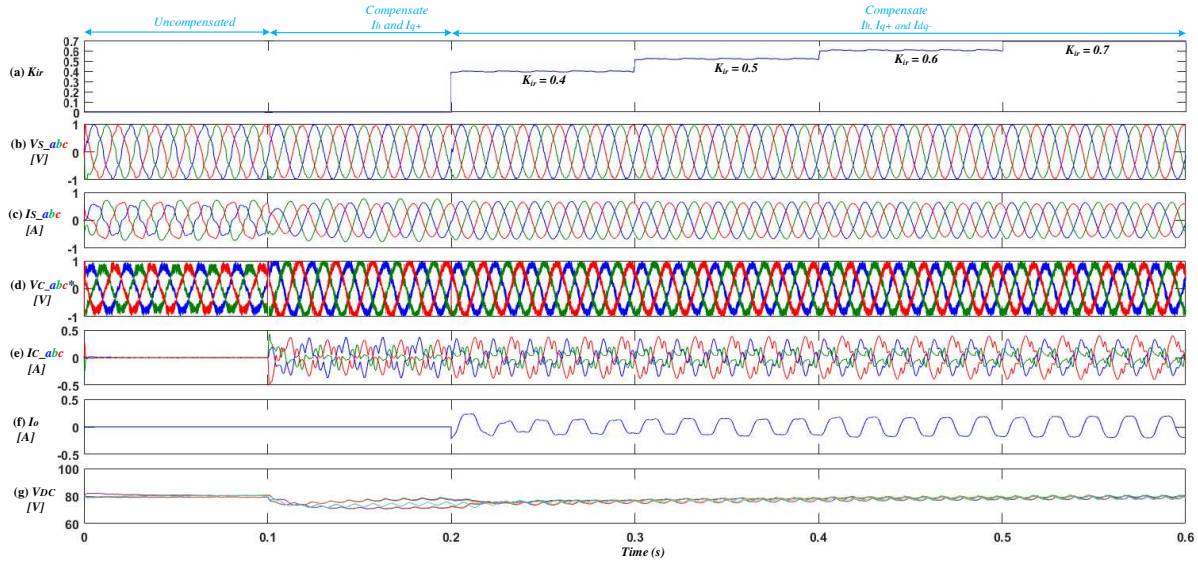

Fig. 15 Operating behaviour of delta-connected MMCC-APC

VII. EXPERIMENTAL VALIDATION

A. Experimental setup

The experimental tests have been carried out in the power electronic laboratory of University of Leeds, UK. A practical three-phase MMCC-APC is shown in Fig. 16, consisting of two series connected 3-level FCC submodule per phase. The complete test system is supplied by the three-phase power supply of 110V 50Hz via a variac, and a three-phase inductor representing the converter filter. The load includes a three-phase R-L load in parallel with three-phase uncontrolled rectifier; the rectifier's phase A input line includes a resistor connected emulating the unbalanced non-linear load, and the three-phase MMCC-APC itself, as shown in Fig. 1. The parameters for this system are same with the simulated system and listed in Table I.

The proposed control strategies shown in Fig. 12 are implemented using a digital signal processor (DSP-TMS320C6713) while the PWM gate signals are generated by a Field Programmable Gate Array (FPGA-ActelProAsic III), as shown in Fig. 16.

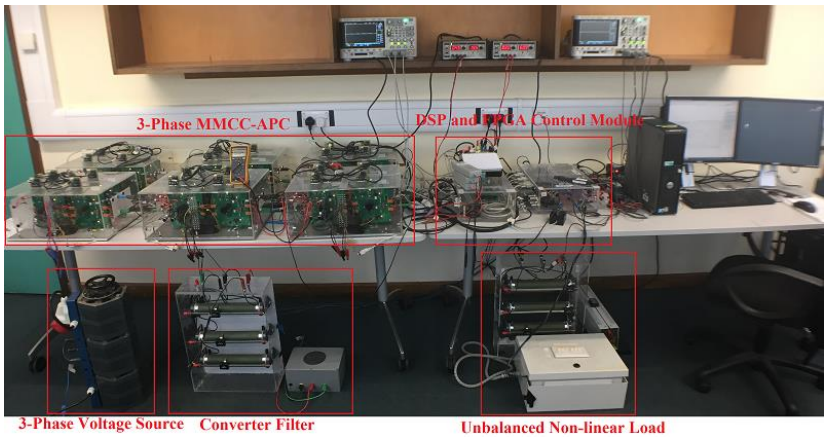

Fig. 16 Laboratory set-up prototype

Fig. 17 shows the results obtained for one case study when K_{ir} = 0.4. With MMCC-APC compensation, the three-phase current and phase A voltage at PCC measured by the oscilloscope are well balanced and giving unity power factor.

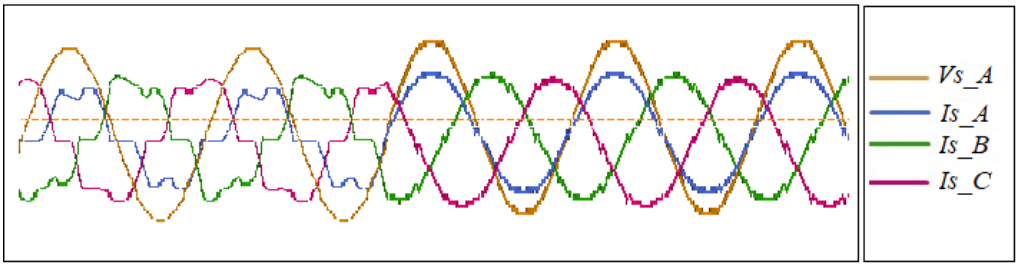

Fig. 17 Compensated and Balanced three-phase PCC current and Phase A source voltage

The following describes tests on the practical MMCC-APC rig, and investigates and compares the operating ranges of this device under the two different control requirements, i.e. compensating reactive power and unbalanced load without harmonic cancellation (Fig. 18), and with harmonic cancellation (Fig. 19). The order of display in both sets of figures is as follows: (a) shows K_{ir} variation, (b) and (c) are waveforms of the supply voltages and currents denoted respectively as V_{Sabc} and I_{Sabc}; Graph (d) shows converter phase cluster reference voltages, V_{Cabc}* and the converter cluster currents, I_{Cabc} are displayed in (e). The imposed zero sequence current for balancing three phase powers denoted as I_o is displayed in (f) and finally the 6 module dc capacitor voltages, V_{DC} are in (g).

B. Without harmonics compensation

In this case, the device functions as a conventional STATCOM by supplying reactive current to the grid according to load drawing value and, if required, may eliminate load current negative sequence element [36]. Fig. 18 displays the results obtained. From 0<t<0.1 second, MMCC-APC is not active, hence the PCC current waveforms shown in Fig. 18(c) are not in phase with the voltage in (b) and unbalanced. At 0.1<t<0.2, reactive current compensation is performed leading to current shown in (c) being in phase with the PCC voltage in (b), but still unbalanced. In this case the converter compensating current, I_{Cabc}, shown in (e) increased. From t>0.2 second, MMCC-APC is set to supply load required reactive current as well as eliminating current imbalanced up to the level measured by K_{ir}= 0.4 to 0.7. During 0.2<t<0.4 when K_{ir} changes from 0.4 to 0.5, the PCC current I_{Sabc} are shown balanced and in phase with V_{Sabc} in (b). The converter terminal current I_{Cabc} (in (e)) is naturally increased and unbalanced while the reference terminal voltage V_{Cabc}* (in (d)) is still balanced. The zero sequence current I_o (in (f)) is increased and 6 module dc voltages (in (g)) are maintained balanced. Further increase K_{ir} to 0.7, the converter controller still performs well and 3-phase supply current is balanced and in phase with PCC voltage. The 6 dc capacitor voltages are still controlled at their nominal value with little ripples.

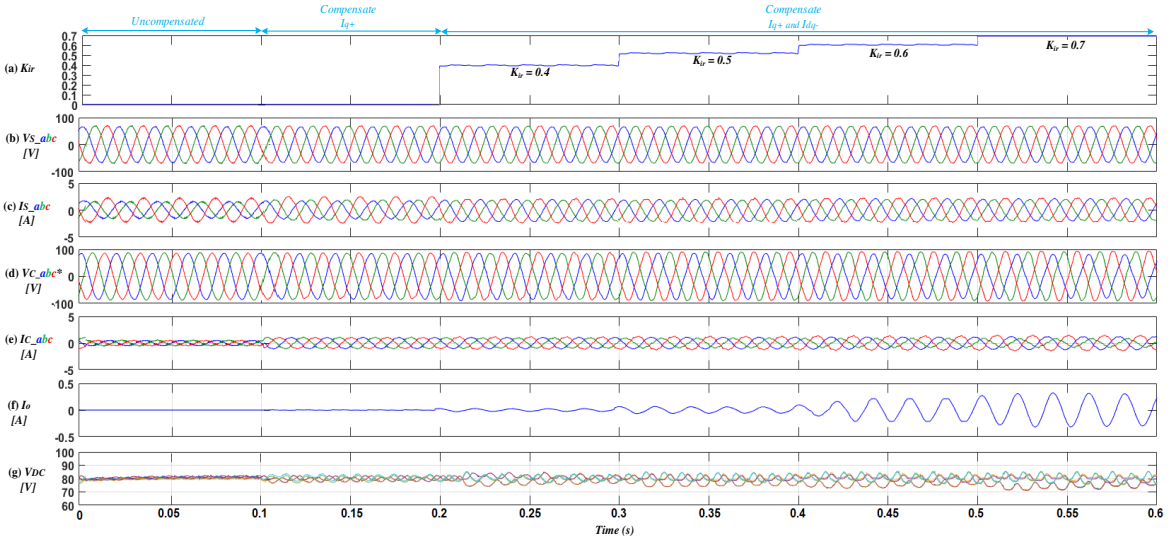

Fig. 18 Compensation of load current imbalance without harmonics

C. With harmonics compensation

When the harmonics compensation function is added to the SDBC-MMCC, the device starts to extract unbalanced harmonics and compensate reactive power. Fig. 19 shows the waveforms of all the variables displayed in the same order as that in Fig. 18 when K_{ir} changes from 0 to 0.7. As can be seen, during time 0<t<0.1second, MMCC-APC does not perform any control, PCC current I_{Sabc} is unbalanced, not in phase with V_{Sabc} in (b) and corrupted with harmonics. From 0.1<t <0.2 second, controller performs both reactive current compensation and harmonic current cancellation, but not to balance the load current. PCC current I_{Sabc} is shown sinusoidal and in phase with V_{Sabc} in (b), but three phase values are unbalanced, hence i_o is zero and V_{DC}s are balanced. V_{Cabc}* is sinusoidal and balanced but I_{Cabc} is shown harmonic distortion since MMCC injects harmonic current to cancel those in the load current. From 0.2<t<0.3 second, MMCC compensates unbalanced current up to K_{ir} =0.4 while simultaneously supplies load reactive current and eliminates harmonics. As can be seen from I_{Sabc} waveforms in (c), good control is obtained, I_{Sabc} is well-balanced with little harmonic corruptions and in phase with the PCC voltage. The converter phase current I_{Cabc} is increased in this case. I_o in (f) is none zero to balance phase cluster voltage. It is distorted due to the compensating of harmonics, but not affects the voltage balancing control. Similar with Fig. 18 case, further increasing K_{ir} to 0.7, PCC current I_{Sabc} can still maintain balanced and sinusoidal, while all the dc capacitor voltages V_{DC}s are maintained at their nominal value.

The ability of delta-connected MMCC-APC control scheme in compensating unbalanced harmonics is clearly shown effective. Comparing the simulated and experimental results, it shows that in both test conditions, the zero sequence current will distorted as long as the device starts to eliminate harmonics current; also, the compensated PCC current waveforms of the experimental results are less ideal than simulation results because that the switching devices and loads are not ideal.

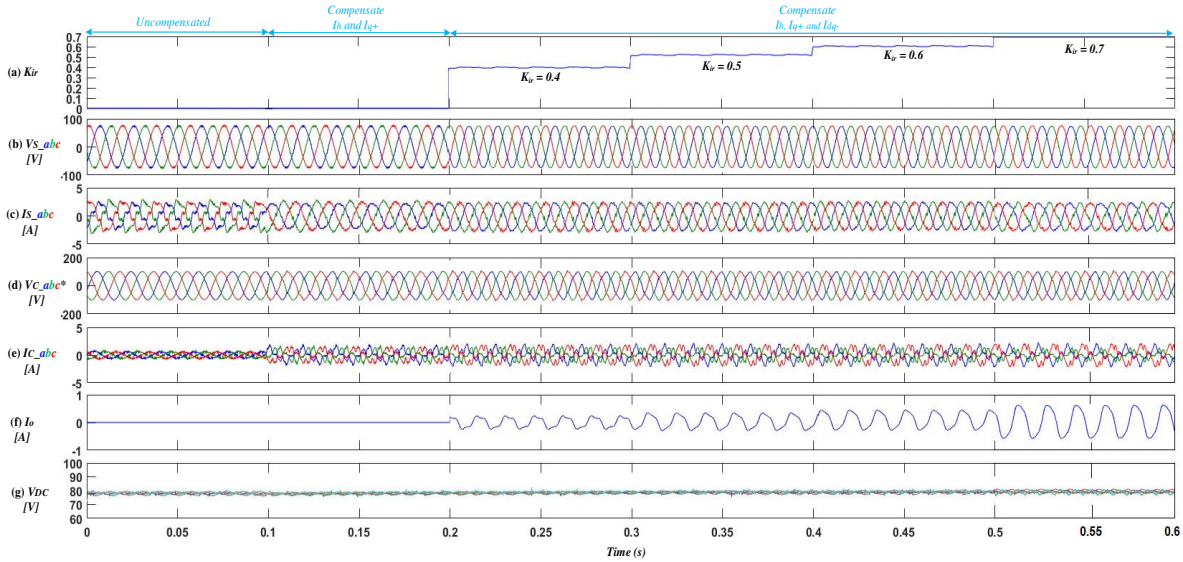

Fig. 19 Compensation of both load current harmonics and imbalance

VIII. CONCLUSIONS

The paper presented a novel control strategy for delta-connected MMCCs to function as active power conditioners which can simultaneously supply load required reactive power, eliminate grid current harmonics and negative sequence current. The contributions of this paper are summarized and shown the following features:

1. Using the proposed cascaded notch filter-based current extraction scheme can eliminate only a selection of dominant low order harmonics hence shows a higher flexibility and faster speed in tracking the harmonic variations. The three-phase grid current using this scheme achieves around 50ms faster of the transient period comparing to conventional Low-pass filter based scheme when load variation occurs.
2. This scheme extracts the negative sequence current and harmonics separately, which avoids the mix of transforming fundamental negative sequence and 3rd order harmonics into 2nd order elements. Hence, it provides higher accuracy and the grid current THDs after compensation are 1% - 5% lower than the Low-pass filter counterpart.
3. The cluster active power of the delta-connected MMCC-APC is controlled to be balanced by injecting a zero sequence current during unbalanced compensation, while the device can compensate up to 1.0 of load unbalance K_{ir}. The simulation and experimental results confirm each other and show that the device can enhance the line current quality effectively.

IX. APPENDIX

Balance and unbalanced harmonic current d-q-0 transformations:

The balanced 3rd harmonic *d-q-0* components derivation:

$$i_0 = \frac{1}{3}(I_3 \cos 3\omega t + I_3 \cos 3\omega t + I_3 \cos 3\omega t) = I_3 \cos 3\omega t \tag{23}$$

$$i_d = \frac{2}{3}\left(I_3 \cos(3\omega t)\sin(\omega t) + I_3 \cos(3\omega t)\sin(\omega t - \tfrac{2\pi}{3}) + I_3 \cos(3\omega t)\sin(\omega t + \tfrac{2\pi}{3})\right) = 0 \tag{24}$$

$$i_q = \frac{2}{3}\left(I_3 \cos(3\omega t)\cos(\omega t) + I_3 \cos(3\omega t)\cos\left(\omega t - \frac{2\pi}{3}\right) + I_3 \cos(3\omega t)\cos\left(\omega t + \frac{2\pi}{3}\right)\right) = 0 \tag{25}$$

The balanced 5th harmonic *d-q-0* components derivation:

$$i_0 = \frac{1}{3}\left(I_5 \cos 5\omega t + I_5 \cos(5\omega t + \tfrac{2\pi}{3}) + I_5 \cos(5\omega t - \tfrac{2\pi}{3})\right) = \frac{1}{3} I_5(0) = 0 \tag{26}$$

$$i_d = \frac{2}{3}\left(I_5 \cos(5\omega t)\sin(\omega t) + I_5 \cos(5\omega t + \tfrac{2\pi}{3})\sin(\omega t - \tfrac{2\pi}{3}) + I_5 \cos(5\omega t - \tfrac{2\pi}{3})\sin(\omega t + \tfrac{2\pi}{3})\right)$$

$$= \frac{2}{3} I_5 \left(\frac{\sin(6\omega t) - \sin(4\omega t)}{2} + \frac{\sin(6\omega t) - \sin(4\omega t + \frac{4\pi}{3})}{2} + \frac{\sin(6\omega t) - \sin(4\omega t - \frac{4\pi}{3})}{2}\right) = I_5 \sin(6\omega t) \tag{27}$$

$$i_q = \frac{2}{3}\left(I_5 \cos(5\omega t)\cos(\omega t) + I_5 \cos(5\omega t + \tfrac{2\pi}{3})\cos(\omega t - \tfrac{2\pi}{3}) + I_5 \cos(5\omega t - \tfrac{2\pi}{3})\cos(\omega t + \tfrac{2\pi}{3})\right)$$

$$= \frac{2}{3} I_5 \left(\frac{\cos(6\omega t) + \cos(4\omega t)}{2} + \frac{\cos(6\omega t) + \cos(4\omega t + \frac{4\pi}{3})}{2} + \frac{\cos(6\omega t) + \cos(4\omega t - \frac{4\pi}{3})}{2}\right) = I_5 \cos(6\omega t) \tag{28}$$

The balanced 7th harmonic *d-q-0* components derivation:

$$i_0 = \frac{1}{3}\left(I_7 \cos 7\omega t + I_7 \cos(7\omega t - \tfrac{2\pi}{3}) + I_7 \cos(7\omega t + \tfrac{2\pi}{3})\right) = \frac{1}{3} I_7(0) = 0 \tag{29}$$

$$i_d = \frac{2}{3}\left(I_7 \cos(7\omega t)\sin(\omega t) + I_7 \cos(7\omega t - \frac{2\pi}{3})\sin(\omega t - \frac{2\pi}{3}) + I_7 \cos(7\omega t + \frac{2\pi}{3})\sin(\omega t + \frac{2\pi}{3})\right)$$

$$= \frac{2}{3} I_7 \left(\frac{\sin(8\omega t) - \sin(6\omega t)}{2} + \frac{\sin\left(8\omega t - \frac{4\pi}{3}\right) - \sin(6\omega t)}{2} + \frac{\sin\left(8\omega t + \frac{4\pi}{3}\right) - \sin(6\omega t)}{2}\right) = -I_7 \sin(6\omega t) \tag{30}$$

$$i_q = \frac{2}{3}\left(I_7 \cos(7\omega t)\cos(\omega t) + I_7 \cos(7\omega t - \tfrac{2\pi}{3})\cos(\omega t - \tfrac{2\pi}{3}) + I_7 \cos(7\omega t + \tfrac{2\pi}{3})\cos(\omega t + \tfrac{2\pi}{3})\right)$$

$$= \frac{2}{3} I_7 \left(\frac{\cos(8\omega t) + \cos(6\omega t)}{2} + \frac{\cos(8\omega t - \frac{4\pi}{3}) + \cos(6\omega t)}{2} + \frac{\cos(8\omega t + \frac{4\pi}{3}) + \cos(6\omega t)}{2}\right) = I_7 \cos(6\omega t) \tag{31}$$

The example unbalanced 3rd harmonic *d-q-0* components derivation:

$$i_0 = \frac{1}{3}(I_3 \cos 3\omega t + I_3 \cos 3\omega t + 0) = \frac{2}{3} I_3 \cos 3\omega t \tag{32}$$

$$i_d = \frac{2}{3}\left(I_3 \cos(3\omega t)\sin(\omega t) + I_3 \cos(3\omega t)\sin(\omega t - \frac{2\pi}{3}) + 0 \times \cos(3\omega t)\sin(\omega t + \frac{2\pi}{3})\right)$$

$$= \frac{2}{3} I_3 \left(\frac{\sin(4\omega t) - \sin(2\omega t)}{2} + \frac{\sin\left(4\omega t - \frac{2\pi}{3}\right) - \sin(2\omega t + \frac{2\pi}{3})}{2} + 0\right)$$

$$= \frac{1}{3} I_3 \left(\sin(4\omega t) - \sin(2\omega t) + \sin\left(4\omega t - \frac{2\pi}{3}\right) - \sin(2\omega t + \frac{2\pi}{3})\right) \tag{33}$$

$$i_q = \frac{2}{3}\left(I_3\cos(3\omega t)\cos(\omega t) + I_3\cos(3\omega t)\cos(\omega t - \frac{2\pi}{3}) + 0 \times \cos(3\omega t)\cos(\omega t + \frac{2\pi}{3})\right)$$

$$= \frac{2}{3}I_3\left(\frac{\cos(4\omega t) + \cos(2\omega t)}{2} + \frac{\cos\left(4\omega t - \frac{2\pi}{3}\right) + \cos\left(2\omega t + \frac{2\pi}{3}\right)}{2} + 0\right)$$

$$= \frac{1}{3}I_3\left(\cos(4\omega t) + \cos(2\omega t) + \cos\left(4\omega t - \frac{2\pi}{3}\right) + \cos\left(2\omega t + \frac{2\pi}{3}\right)\right) \quad (34)$$

X. REFERENCES

[1] J. M. Carrasco *et al.*, "Power-electronic systems for the grid integration of renewable energy sources: A survey," *IEEE Transactions on Industrial Electronics, 53 (4), 1002-1016.,* 2006.

[2] J. P. Painuly, "Barriers to renewable energy penetration; a framework for analysis," *Renewable Energy,* vol. 24, no. 1, pp. 73-89, 2001.

[3] B. Singh, S. Murthy, and R. S. R. Chilipi, "STATCOM-based controller for a three-phase SEIG feeding single-phase loads," *IEEE Transactions on Energy Conversion,* vol. 29, no. 2, pp. 320-331, 2014.

[4] J. A. Muñoz, J. R. Espinoza, C. R. Baier, L. A. Morán, J. I. Guzman, and V. M. Cárdenas, "Decoupled and modular harmonic compensation for multilevel STATCOMs," *IEEE Transactions on Industrial Electronics,* vol. 61, no. 6, pp. 2743-2753, 2014.

[5] J. Das, "Application of STATCOM to an industrial distribution system connected to a weak utility system," *IEEE Transactions on Industry Applications,* vol. 52, no. 6, pp. 5345-5354, 2016.

[6] M. Hagiwara and H. Akagi, "Control and experiment of pulsewidth-modulated modular multilevel converters," *IEEE Transactions on Power Electronics,* vol. 24, no. 7, pp. 1737-1746, 2009.

[7] S. Debnath, J. Qin, B. Bahrani, M. Saeedifard, and P. Barbosa, "Operation, control, and applications of the modular multilevel converter: A review," *IEEE Transactions on Power Electronics,* vol. 30, no. 1, pp. 37-53, 2015.

[8] H. Akagi, "Classification, terminology, and application of the modular multilevel cascade converter (MMCC)," *IEEE Transactions on Power Electronics,* vol. 26, no. 11, pp. 3119-3130, 2011.

[9] M. Saeedifard and R. Iravani, "Dynamic performance of a modular multilevel back-to-back HVDC system," *IEEE Transactions on Power Delivery,* vol. 25, no. 4, pp. 2903-2912, 2010.

[10] J. Peralta, H. Saad, S. Dennetière, J. Mahseredjian, and S. Nguefeu, "Detailed and averaged models for a 401-level MMC–HVDC system," *IEEE Transactions on Power Delivery,* vol. 27, no. 3, pp. 1501-1508, 2012.

[11] A. Nami, J. Liang, F. Dijkhuizen, and G. D. Demetriades, "Modular multilevel converters for HVDC applications: Review on converter cells and functionalities," *IEEE Transactions on Power Electronics,* vol. 30, no. 1, pp. 18-36, 2015.

[12] E. Kontos, G. Tsolaridis, R. Teodorescu, and P. Bauer, "High order voltage and current harmonic mitigation using the modular multilevel converter statcom," *IEEE Access,* vol. 5, pp. 16684-16692, 2017.

[13] J. Li, G. Konstantinou, H. R. Wickramasinghe, and J. Pou, "Operation and control methods of modular multilevel converters in unbalanced ac grids: A review," *IEEE Journal of Emerging and Selected Topics in Power Electronics,* 2018.

[14] L. Zhang, Y. Tang, S. Yang, and F. Gao, "Decoupled power control for a modular-multilevel-converter-based hybrid AC–DC grid integrated with hybrid energy storage," *IEEE Transactions on Industrial Electronics,* vol. 66, no. 4, pp. 2926-2934, 2019.

[15] P. H. W. a. P. T. Cheng, "A Fault Tolerant Control Strategy for the Delta-Connected Cascaded Converter,," *IEEE Transactions on Power Electronics,* vol. 99, p. 1, 2018.

[16] O. J. K. Oghorada and L. Zhang, "Unbalanced and Reactive Load Compensation Using MMCC-Based SATCOMs With Third-Harmonic Injection," *IEEE Transactions on Industrial Electronics,* vol. 66, no. 4, pp. 2891-2902, Apr 2019.

[17] H.-C. Chen, P.-H. Wu, C.-T. Lee, C.-W. Wang, C.-H. Yang, and P.-T. Cheng, "Zero-sequence voltage injection for dc capacitor voltage balancing control of the star-connected cascaded H-bridge PWM converter under unbalanced grid," *IEEE Transactions on Industry Applications,* vol. 51, no. 6, pp. 4584-4594, 2015.

[18] H. Akagi, S. Inoue, and T. Yoshii, "Control and performance of a transformerless cascade PWM STATCOM with star configuration," *IEEE Transactions on Industry Applications,* vol. 43, no. 4, pp. 1041-1049, 2007.

[19] Q. Song and W. Liu, "Control of a cascade STATCOM with star configuration under unbalanced conditions," *IEEE Transactions on Power Electronics,* vol. 24, no. 1, pp. 45-58, 2009.

[20] P.-H. Wu, H.-C. Chen, Y.-T. Chang, and P.-T. Cheng, "Delta-connected cascaded H-bridge converter application in unbalanced load compensation," *IEEE Transactions on Industry Applications,* vol. 53, no. 2, pp. 1254-1262, 2017.

[21] J.-J. Jung, J.-H. Lee, S.-K. Sul, G. T. Son, and Y.-H. Chung, "DC Capacitor Voltage Balancing Control for Delta-Connected Cascaded H-Bridge STATCOM Considering Unbalanced Grid and Load Conditions," *IEEE Transactions on Power Electronics,* vol. 33, no. 6, pp. 4726-4735, 2018.

[22] A. Massoud, S. Finney, and B. Williams, "Review of harmonic current extraction techniques for an active power filter," in *2004 11th International Conference on Harmonics and Quality of Power (IEEE Cat. No. 04EX951)*, 2004, pp. 154-159: IEEE.

[23] W. M. Grady, M. J. Samotyj, and A. H. Noyola, "Survey of active power line conditioning methodologies," *IEEE Transactions on Power Delivery,* vol. 5, no. 3, pp. 1536-1542, 1990.

[24] A. A. Girgis, W. B. Chang, and E. B. Makram, "A digital recursive measurement scheme for online tracking of power system harmonics," *IEEE Transactions on Power Delivery,* vol. 6, no. 3, pp. 1153-1160, 1991.

[25] H. Akagi, Y. Kanazawa, and A. Nabae, "Instantaneous reactive power compensators comprising switching devices without energy storage components," *IEEE Transactions on Industry Applications,* no. 3, pp. 625-630, 1984.

[26] H. Akagi, E. H. Watanabe, and M. Aredes, *Instantaneous power theory and applications to power conditioning*. John Wiley & Sons, 2017.

[27] F. Z. Peng, G. W. Ott, and D. J. Adams, "Harmonic and reactive power compensation based on the generalized instantaneous reactive power theory for three-phase four-wire systems," *IEEE Transactions on Power Electronics,* vol. 13, no. 6, pp. 1174-1181, 1998.

[28] M. Pradhan and M. K. Mishra, "Dual *P-Q* Theory Based Energy-Optimized Dynamic Voltage Restorer for Power Quality Improvement in a Distribution System," *IEEE Transactions on Industrial Electronics,* vol. 66, no. 4, pp. 2946-2955, 2019.

[29] K. Takagi and H. Fujita, "A three-phase grid-connected inverter equipped with a shunt instantaneous reactive power compensator," *IEEE Transactions on Industry Applications,* 2019.

[30] S. Bhattacharya and D. Divan, "Synchronous frame based controller implementation for a hybrid series active filter system," in *IAS'95. Conference Record of the 1995 IEEE Industry Applications Conference Thirtieth IAS Annual Meeting*, 1995, vol. 3, pp. 2531-2540: IEEE.

[31] R. Teodorescu, M. Liserre, and P. Rodriguez, *Grid converters for photovoltaic and wind power systems*. John Wiley & Sons, 2011.

[32] M. Hagiwara, R. Maeda, and H. Akagi, "Negative-sequence reactive-power control by a PWM STATCOM based on a modular multilevel cascade converter (MMCC-SDBC)," *IEEE Transactions on Industry Applications,* vol. 48, no. 2, pp. 720-729, 2011.

[33] J. A. Barrena, L. Marroyo, M. Á. R. Vidal, and J. R. T. Apraiz, "Individual voltage balancing strategy for PWM cascaded H-bridge converter-based STATCOM," *IEEE Transactions on Industrial Electronics,* vol. 55, no. 1, pp. 21-29, 2008.

[34] R. Naderi and A. Rahmati, "Phase-shifted carrier PWM technique for general cascaded inverters," *IEEE Transactions on Power Electronics,* vol. 23, no. 3, pp. 1257-1269, 2008.

[35] H. Huang, O. K. Oghorada, L. Zhang, and B. Chong, "Active harmonic current elimination and reactive power compensation using modular multilevel cascaded converter," in *2017 19th European Conference on Power Electronics and Applications (EPE'17 ECCE Europe)*, 2017, pp. P. 1-P10: IEEE.

[36] O. Oghorada and L. Zhang, "Analysis of star and delta connected modular multilevel cascaded converter-based STATCOM for load unbalanced compensation," *International Journal of Electrical Power & Energy Systems,* vol. 95, pp. 341-352, 2018.